Photodissociation Reaction of 1,2-Diiodoethane in Solution: A Theoretical and X-ray Diffraction Study

Qingyu Kong,*,† Joonghan Kim,‡ Maciej Lorenc,† Tae Kyu Kim,‡ Hyotcherl Ihee,*,‡ and Michael Wulff†

European Synchrotron Radiation Facility, Grenoble Cedex 38043, BP 220, France, and Department of Chemistry and School of Molecular Science (BK21), Korea Advanced Institute of Science and Technology (KAIST), Daejeon 305-701, Republic of Korea

Received: June 22, 2005; In Final Form: August 16, 2005

Various molecular species are known to form during the photoreaction of $C_2H_4I_2$ in the gas phase and in solution. We have studied all species involved in this reaction by ab initio and density functional theory (DFT) calculations: Geometries, energies, and vibrational frequencies of $C_2H_4I_2$, bridged $C_2H_4I\bullet$, anti $C_2H_4I\bullet$, C_2H_4, I_2, I_3^-, and the isomer C_2H_4I-I were calculated. The absorption peaks and oscillator strengths of selected species along the potential energy surface (PES) were calculated using time-dependent DFT and were compared with available experimental results. The calculated PES satisfactorily describes the observed reactions of the photoexcited $C_2H_4I_2$ molecule. In the gas phase, there is only one reaction pathway: the first C−I bond ruptures followed by a secondary C−I breakage in the haloethyl radical $C_2H_4I\bullet$. In solution, by contrast, another reaction channel, which is energetically more favored over the secondary dissociation, is switched on due to a solvation effect: the bridged $C_2H_4I\bullet$ can bind to the free iodine atom to form a C_2H_4I-I isomer without any energy barrier. The isomer can then break into C_2H_4 and I_2. The rotational barriers in the gas phase and in solution were also calculated and compared. To provide experimental data on the structure of $C_2H_4I_2$ in solution, the ground state structure of $C_2H_4I_2$ in methanol was determined from static X-ray diffraction data using 88 keV ($\lambda = 0.14$ Å) X-rays. The structural parameters are compared with those from the theoretical results.

1. Introduction

The structure of small molecules (i.e., the time and space averaged positions of all atoms) in the gas phase can be readily studied by electron diffraction. Similar information can be obtained in a straightforward manner for the solid state if crystals are available. In contrast, the structures in disordered phases such as solutions are difficult to study and at this stage no routine methods are available to determine averaged local structures in solution. Here, we used static diffraction of 88 keV X-rays to determine the structure of $C_2H_4I_2$ when dissolved in methanol.

1,2-Disubstituted ethane $C_2H_4X_2$ molecules and haloethyl radicals $C_2H_4X\bullet$ (X = F, Cl, Br, and I) have been thoroughly investigated in stereochemical,[1−7] thermochemical, and photochemical studies.[8−18] Since interesting aspects of the stereochemistry are observed in 1,2-dihalocompounds, many fundamental questions in conformational analysis were addressed by the study of 1,2-disubstituted ethanes,[19] which are "structural prototypes", the simplest structures that incorporate functional groups commonly found in larger systems.

The iodoethyl compounds have been extensively studied by time-resolved electron and X-ray diffraction experiments due to the high *Z*-number of iodine.[20−22] However, there are few theoretical studies on iodine containing molecules,[23−25] as they present higher computational complexity. We have recently investigated the photodissociation process of $C_2H_4I_2$ in methanol by time-resolved X-ray diffraction and confirmed the existence of the bridged $C_2H_4I\bullet$ radical.[26] Here, we present quantum chemical calculations for photoinduced reactions and putative photoproducts of dissociated $C_2H_4I_2$, to get a more detailed picture of the dissociation mechanism in solution. Static X-ray diffraction measurements of the ground state structure of $C_2H_4I_2$ in methanol are also shown and compared with the calculation.

2. Experimental and Computational Methods

2.1. Static X-ray Diffraction. The basic formulas used to determine the ground state molecular structure from the scattered X-ray signal are summarized in this section.[27,28] The scattered intensity is generally expressed as a function of $q = (4\pi/\lambda)\sin(2\theta/2)$, where λ is the X-ray wavelength and 2θ is the scattering angle.

The total diffraction signal from a liquid is generally described in terms of partial structure factors which are related to the Fourier transform of the statistical correlation between scattering sites, $g(r)$.[29] In the present study, with very hard (88 keV) X-rays, the effective $g(r)$ is dominated by the contributions from heavy atoms and is related to the scattering signal:

$$S(q) = f_e^2(q) + f_e^2(q)\int 4\pi r^2\rho(g(r) - 1)\frac{\sin(qr)}{qr}\,dr \quad (1)$$

where ρ is the atomic number density for the material under study and f_e is an average scattering factor per electron:

$$f_e = (\sum_{uc} f_m)/\sum_{uc} Z_m \quad (2)$$

* To whom correspondence should be addressed. E-mail: kong@esrf.fr (Q.K.); hyotcherl.ihee@kaist.ac.kr (H.I.).
† European Synchrotron Radiation Facility.
‡ Korea Advanced Institute of Science and Technology (KAIST).

10.1021/jp053390q CCC: $30.25
Published on Web 10/22/2005

Here, f_m is the elastic scattering factor for atom m, uc is the unit of composition or unit cell, and Z is the number of electrons of atom m. The back transform yields

$$g(r) = 1 + \frac{1}{2\pi^2\rho r}\int \frac{q(S(q) - f_e^2(q))}{f_e^2(q)} \sin(qr)e^{-(\alpha q)^2}\, dq \quad (3)$$

$S(q) - f_e^2(q)$ represents the deviation from atomic scattering due to interference, and the integrals range from zero to infinity. In practice, the termination effects due to the finite q-range of the experiment are attenuated by using an exponential damping factor, α. ρ is the atomic number density. Here, $g(r)$ is a measure of the electron density seen from the center of an average atom. Strictly speaking, eq 1 is valid for systems containing only one type of atom. For a system containing more than one kind of atom, this equation is an approximation. Therefore, eq 3 is also an approximation, weighted toward heavy atom contribution in proportion to Z^2.

The total diffraction signal, $S(q)$, from $C_2H_4I_2$ in methanol can be expressed as the sum of different contributions from solute, solvent, and solute−solvent interaction:[30]

$$S(q)_{solution} = S(q)_{solute} + S(q)_{solvent} + S(q)_{solute-solvent} \quad (4)$$

Because both the elastic and inelastic signals are detected in the static X-ray diffraction experiments, the latter was also included in the calculation.[31]

To extract the ground state structure of $C_2H_4I_2$, the experimental data were processed in the following way: (a) First, the pure solvent scattering, $S(q)_{solvent}$, was subtracted from the total scattering of the solution, $S(q)_{solution}$, and the difference signal, $S(q)_{solute} + S(q)_{solute-solvent}$, was then scaled to the average gas scattering factor of $C_2H_4I_2$, f_e^2, and corrected by the calculated Compton scattering of the solute. (b) Second, f_e^2 of $C_2H_4I_2$ was subtracted from the experimental difference data, $S(q)_{solute} + S(q)_{solute-solvent}$. The remaining data contain two terms: $S(q)_{solute-solvent}$, the cage structure, and the interference terms from atom−atom pairs, $\sin(qr_{ij})/qr_{ij\ (i\neq j)}$, molecular structure of the solute. (c) To bring out the oscillations at high q, the remaining signal, designated as $S(q)_{structure} = S(q)_{solute} + S(q)_{solute-solvent} - f_e^2(q)$, was multiplied by q and divided by the sharpening function, $\sum f_i^2(q)$. Although all structural information is contained in the molecular scattering function, $S(q)_{structure}$, the radial distribution function, $g(r)_{structure}$, is more intuitive for qualitative interpretation, as it directly reflects the relative density of internuclear distance in the molecule. When the sharpening function is taken into account, the final $g(r)_{structure}$ function takes the following form:

$$g(r)_{structure} = 1 + \frac{1}{2\pi^2\rho r}\int_0^{+\infty} \frac{qS(q)_{structure}}{\sum f_i^2(q)} \sin(qr)e^{-(\alpha q)^2}\, dq \quad (5)$$

2.2. Ab Initio and Density Functional Theory (DFT) Computations. Calculations were carried out by ab initio and DFT methods using the Gaussian 03 code.[32] Geometries were fully optimized, vibrational frequencies were calculated with analytical second-order derivatives, and zero-point vibrational energies were derived. The number of imaginary frequencies was used to characterize the nature of the structure. For the transition state, intrinsic reaction coordinate (IRC) calculations were performed to follow the reaction path. The structural parameters were also optimized with the coupled cluster CCSD(T) method[33] for comparison.

TABLE 1: Calculated Bond Lengths of I_2 in the Gas Phase with Different Basis Sets at the HF and B3LYP Levels

	I_2 bond length (Å)	
basis set	B3LYP	HF
3-21G**	2.719	2.696
6-31+G	2.732	2.700
6-311G	2.859	2.810
6-311G(d)	2.737	2.703
6-311+G(d)	2.707	2.676
Lanl2dz	2.863	2.817
experiment[41]	2.67 ± 0.004	

The Becke three-parameter hybrid functional with the Lee−Yang−Parr correlation corrections (B3LYP) was used in the DFT calculation.[34,35] The all-electron basis set 6-311++G(d,p) for C and H atoms[36] and the all-electron basis sets 6-311G(d) with added d and f polarization functions and s and p diffuse functions for the I atom,[37,38] which are referred to as 6-311+G-(d), were used. For the geometry of the anti $C_2H_4I\bullet$ radical, the Hartree−Fock (HF) and MP2 results were used, since the anti form converged to the bridged structure in DFT and CCSD(T) calculations. For all other structures, the DFT results are presented.

The solvent effects were calculated using self-consistent reaction field (SCRF) theory. The Self-Consistent Isodensity Polarized Continuum Model (SCIPCM),[39] which allows geometry optimization at the HF and DFT levels, was used to perform the solution calculation using an isodensity value of 0.0004 e/au^3 for both methanol and cyclohexane solutions.

Time-dependent density functional theory (TD-DFT)[40] was used to calculate the vertical excitation energies, oscillator strengths, and excited potential energy surfaces. The TD-B3LYP method with the same basis sets for C, H, and I atoms as described above was used in these calculations. To obtain the excited potential energy curves, the single-point energies were calculated at each point of the ground state surface. In the calculation, the C_s symmetry rather than the C_{2h} symmetry of optimized ground state geometry was preserved.

To choose an appropriate basis set for the iodine atom, the bond length of the I_2 molecule was calculated with different basis sets and compared to the experimental gas phase value 2.67 ± 0.004 Å.[41] The calculated results at HF and B3LYP levels are shown in Table 1, and the all-electron 6-311+G(d) basis set was finally chosen for iodine.

3. Results and Discussion

In section 3.1, the static X-ray diffraction results of the ground state structure of 1,2-diiodoethane in methanol are presented. In section 3.2, we will discuss the rotational potential energy surface of 1,2-diiodoethane around the C−C axis in solution and the gas phase, and in section 3.3, we will present various dissociation channels for photoinduced chemical reactions.

3.1. Static X-ray Diffraction. The diffraction experiments were carried out on the high-energy beamline ID15 with 88 keV (0.141 Å) X-rays. The higher energy extended the q-range up to 23 Å^{-1}, which correspondingly improves the spatial resolution to ~0.27 Å. The 60 mM $C_2H_4I_2/CH_3OH$ solution, which translates to a solute−solvent ratio of 1:412, was used in the X-ray diffraction experiments. The samples were purchased from Sigma-Aldrich and used without further purification. The $C_2H_4I_2/CH_3OH$ solution was added into a 3 mm thick capillary, and the scattering signal was integrated on a 2300 × 2300 pixel image plate with a pixel size of 150 μm.

Figure 1a shows the total scattering intensity from the $C_2H_4I_2/CH_3OH$ solution, $S(q)_{solution}$, and Figure 1b shows the scattering

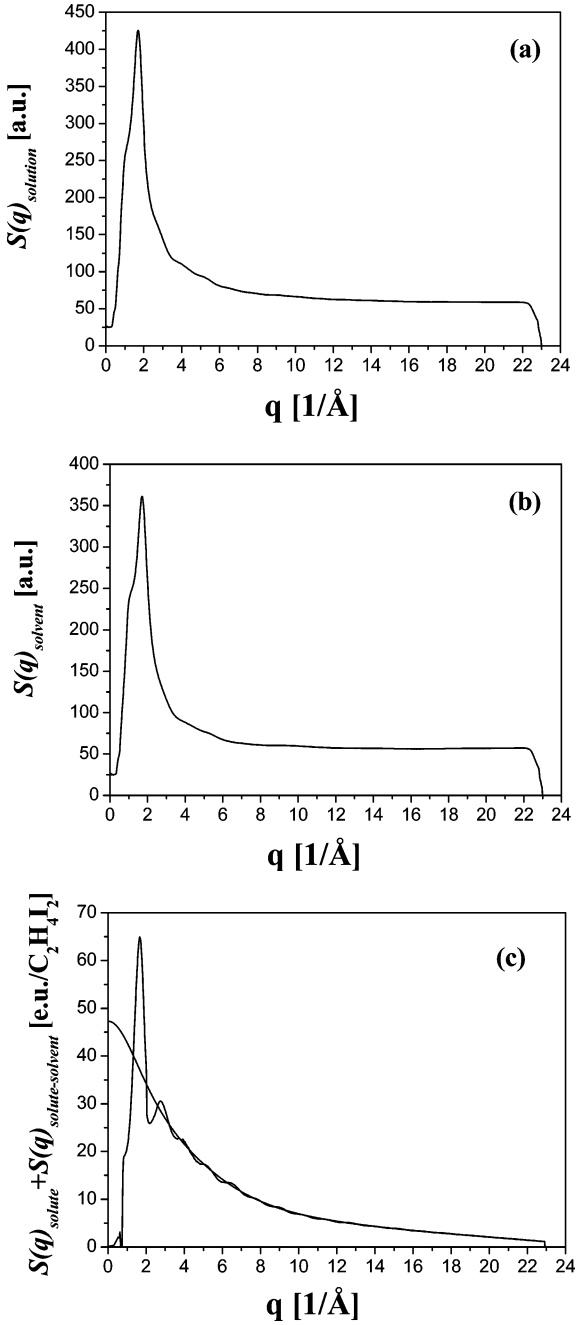

Figure 1. Static X-ray diffraction of $C_2H_4I_2$ in methanol: (a) the total scattered intensity from $C_2H_4I_2$ in methanol, $S(q)_{solution}$; (b) scattered intensity from pure methanol, $S(q)_{solvent}$; (c) scaling of the difference between $C_2H_4I_2$ in methanol and pure methanol, $S(q)_{solute} + S(q)_{solute-solvent}$, to the average gas scattering factor of $C_2H_4I_2$, f_e^2.

intensity from pure methanol, $S(q)_{solvent}$. After subtracting the pure solvent scattering from the total scattering of the solution, the difference signal, $S(q)_{solute} + S(q)_{solute-solvent}$, was scaled to the average gas scattering factor of $C_2H_4I_2$, f_e^2, as shown in Figure 1c. Figure 2 shows the structure of $C_2H_4I_2$ in q- and real spaces. Figure 2a was obtained by subtracting f_e^2 of $C_2H_4I_2$ from $S(q)_{solute} + S(q)_{solute-solvent}$ and multiplying it by $q/\sum f_i^2(q)$. Fourier sine transform of the curve in Figure 2a, according to eq 5, leads to the radial distribution curve in Figure 2b, which represents the molecular structure of the solute, $C_2H_4I_2$.

The interatomic distances in Figure 2b are assigned as follows: the first peak around 1 Å is an artifact caused by the absence of experimental data close to $q = 0$, the inevitable consequence of using a beamstop; the peak at 2.2 Å is the

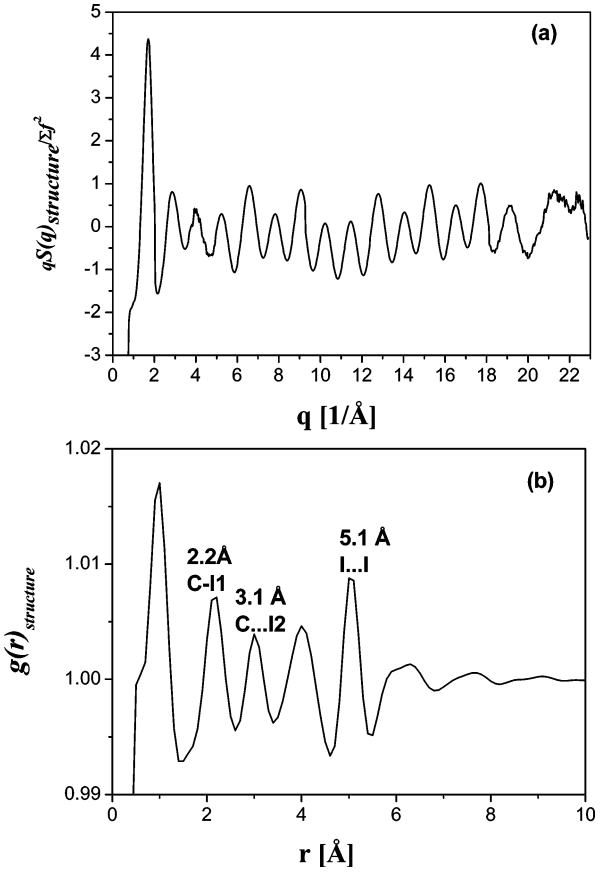

Figure 2. Structure of $C_2H_4I_2$ in methanol: (a) $qS(q)_{structure}/\sum f_i^2(q)$, where $S(q)_{structure}$ is obtained after subtraction of f_e^2 for $C_2H_4I_2$ from $S(q)_{solute} + S(q)_{solute-solvent}$; (b) $g(r)_{structure}$.

covalent C−I bond; the peak at 3.1 Å is the (nonbonded) C···I distance; the peak at 5.1 Å is the (nonbonded) I···I distance. The broad peak around 4.0 Å is tentatively assigned to the first solvation shell.

3.2. Rotational Potential Energy Surfaces. To observe the effect of solvation of the $C_2H_4I_2$ molecule on the rotational potential energy surface, we calculated the potential energy as a function of the torsion angle around the C−C axis in the gas phase as well as in solution. The calculation was performed at the B3LYP level, the geometries of the minima and the transition structures were fully optimized, and the vibrational frequencies were calculated. Figure 3 shows the rotational energy curves in the gas phase, in cyclohexane, and in methanol using the SCIPCM model. The total and relative energies at the minima and the transition states are given in Supporting Information Table 1S. The optimized structures in the gas phase and in methanol are presented in Figure 4, and the detailed geometrical parameters of the optimized structures as well as the calculated vibrational frequencies in the gas phase and in methanol are listed in Supporting Information Tables 2S and 3S.

The solvent effect on $C_2H_4I_2$ along the rotational potential energy surface (PES) is clearly illustrated in Figure 3: the solute−solvent interaction stabilizes the solute. In the SCRF theory, the solvent is considered as a continuum reaction field with uniform dielectric constant ϵ and the solute is placed in a cavity in the solvent. The interaction between the solute and solvent depends on the properties of both the solvent, represented by the dielectric constant, and the solute represented by dipole and multipole moments. Thus, methanol with a large dielectric constant of 32.63 is expected to have a more stabilizing effect on the solute molecule than cyclohexane with a smaller

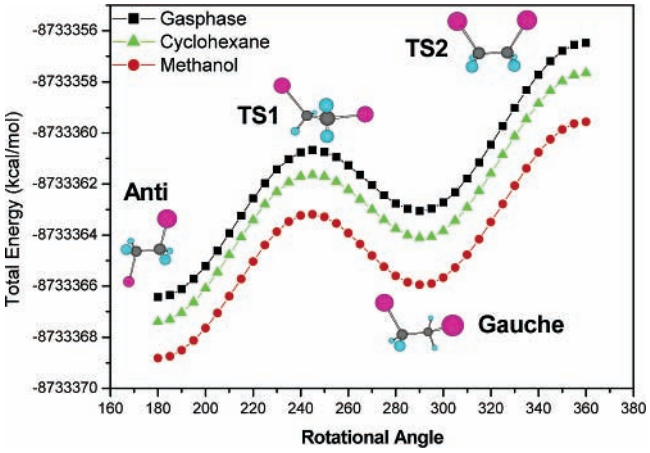

Figure 3. Rotational potential energy curves for the $C_2H_4I_2$ molecule around the dihedral angle ICCI, in the gas phase, in cyclohexane, and in methanol, calculated at the B3LYP level. The all-electron 6-311++G-(d,p) basis set for the C and H atoms and the 6-311+G(d) basis set for iodine were used. The SCIPCM model was used for calculations in the solution phase.

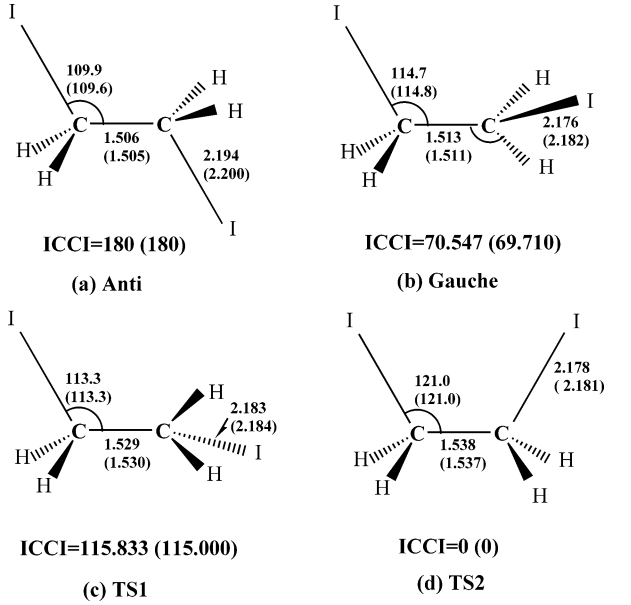

Figure 4. Geometries of $C_2H_4I_2$: (a) anti form; (b) gauche form; (c) transition state 1 (TS1 anti → gauche); (d) transition state 2 (TS2 gauche → gauche) calculated at the B3LYP level (distances in angstroms and angles in degrees). ICCI indicates the dihedral angle. The values in parentheses show the structural parameters in methanol. Detailed structural parameters are shown in Supporting Information Table 2S.

dielectric constant of 2.023. The difference between methanol and cyclohexane is demonstrated in Figure 3. For the anti form, the energy difference between the gas phase and methanol is 2.372 kcal/mol, while, for cyclohexane, it is only 0.935 kcal/mol (Supporting Information Table 1S). According to the reaction field theory, the solvent effect in cyclohexane, compared to the gas phase, will be about 40% of that in a high-dielectric-constant solvent, and our results confirm this.[42]

We noticed that the relative energy between the anti and gauche forms decreases from 3.232 kcal/mol in the gas phase to 2.617 kcal/mol in methanol. The smaller energy difference in solution means that the solvent interacts more strongly with the gauche form than with the anti form. This is because the interaction between the solute and the solvent depends not only on the polarizability of the solvent but also on the dipole and multipole moments of the solute. The anti form of diiodoethane

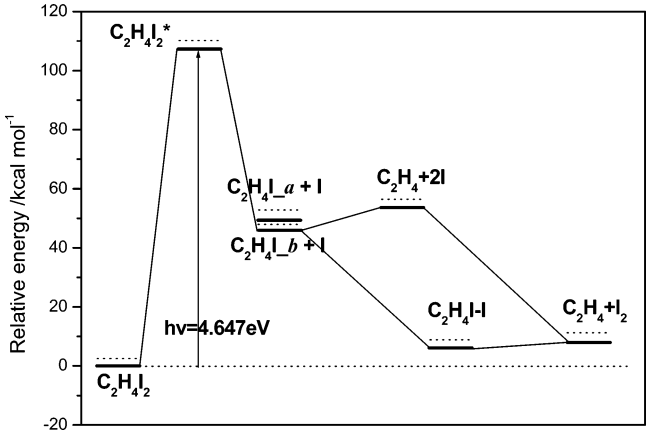

Figure 5. Potential energy levels of the photodissociation of $C_2H_4I_2$ in methanol, plotted using energies calculated at the B3LYP level, 6-311++G(d,p) basis set for C and H, and the 6-311+G(d) basis set for I. $C_2H_4I\_a$ and $C_2H_4I\_b$ stand for the anti and bridged C_2H_4I, respectively. The SCIPCM model is used to include the solvent effect. All energies were subjected to ZPE correction. Dotted lines show the corresponding energy levels in the gas phase.

has C_{2h} symmetry with a dipole moment of zero, whereas the gauche form has C_2 symmetry and a dipole moment of 2.47 D. Therefore, the gauche form of $C_2H_4I_2$ will be more stabilized than its anti form, resulting in decreased relative energy in methanol. The solvent effects are also reflected in the changes of the structural parameters shown in Supporting Information Table 2S, as well as in the changes of the vibrational frequencies (Supporting Information Table 3S).

Our time-resolved[26] and static X-ray scattering results for $C_2H_4I_2$ in methanol show that the gauche form is almost absent within experimental error. This observation is in agreement with the calculated energy difference of 2.617 kcal/mol between the anti and gauche forms in methanol, since, at this energy difference, the gauche population is less than 1% at 300 K. The measured nonbonded I···I distance of 5.1 Å, as shown in Figure 2b, is in good agreement with the calculated value of 5.105 Å for the anti conformer, and not with 4.034 Å for the gauche conformer.

3.3. Dissociation Potential Energy Surfaces. *Bridged and Anti Conformers of C_2H_4I•.* The overall potential energy levels of various candidate species along the photoreaction pathways of $C_2H_4I_2$ are shown in Figure 5. Starting from the hot $C_2H_4I_2$* molecule, the first step in dissociation is to form C_2H_4I• + I•. The bridged and anti conformers of the haloethyl radical C_2H_4I• were first calculated using the HF, MP2, B3LYP, and CCSD-(T) methods in the gas phase, and based on these results, the calculations were extended to solution at the HF and B3LYP levels with the SCIPCM model. The structures of the anti and bridged forms of C_2H_4I• are shown in Figure 6. The selected optimized geometrical parameters are presented in Table 2, and the relative energies are listed in Table 3. The detailed structural parameters and the *XYZ* coordinates of the C_2H_4I• radical with bridged and anti conformers are shown in Supporting Information Table 4S. The calculated vibrational frequencies for the gas phase and for methanol are shown in Supporting Information Table 5S.

At the B3LYP and CCSD(T) levels, the anti form converged to the bridged form. The calculated C−I bond length in the bridged form is 3.107 Å in methanol at the B3LYP level, in good agreement with the experimental value 3.06 ± 0.02 Å obtained from time-resolved X-ray diffraction.[26] The calculation at the Restricted Open-Shell Hartree−Fock (ROHF) level gave a C−I bond length of 4.144 Å, indicating that the ROHF method

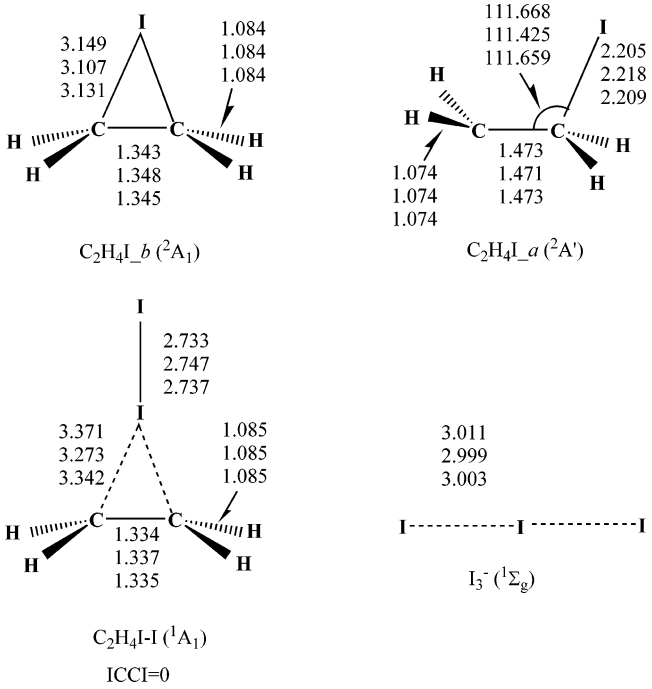

Figure 6. Geometries of C_2H_4I•_b ($^2A_1$), C_2H_4I•_a ($^2A'$), C_2H_4I-I ($^1A_1$) isomer, and I_3^- ($^1\Sigma_g$). Selected geometric parameters in the gas phase, in methanol, and in cyclohexane at the B3LYP level are shown sequentially; bond lengths are in angstroms, and angles are in degrees. Geometric parameters of the anti form of C_2H_4I• are calculated at the ROHF level. ICCI indicates the dihedral angle. The detailed structural parameters and *XYZ* coordinates are shown in Supporting Information Table 4S.

does not describe the bridged C_2H_4I• radical properly. In the gas phase, the C−I bond length in the bridged C_2H_4I•, optimized at the ROHF, MP2, B3LYP, and CCSD(T) levels, is 4.138, 3.129, 3.149, and 3.285 Å, respectively. The MP2 and B3LYP methods produce reasonable results, while the CCSD(T) method slightly overestimates the C−I bond length. The effect of solvation on the molecular geometry is shown in Table 2: the change in the C−I bond length of bridged C_2H_4I• in going from the gas phase to methanol and cyclohexane is 0.042 and 0.018 Å, respectively, at the B3LYP level, which shows again that the effect of cyclohexane is ∼40% of that of methanol.[42]

While the anti form of C_2H_4I• converged to the bridged form at the B3LYP level, the optimization in solution can only be performed at the HF and B3LYP levels. Thus, the relative energy between the bridged and anti forms in optimized geometries in solution is only available at the HF level, as shown in Table 3. The relative energy of 7.985 kcal/mol in the gas phase and 7.391 kcal/mol in methanol at the HF level may overestimate the real energy difference. As discussed above, the HF method cannot produce geometrical parameters for the bridged form appropriately. Single-point energies in the gas phase and in solution at the CCSD(T) level are calculated on the basis of the gas phase geometries of the bridged and anti forms obtained with the MP2 method. The optimized relative energy at the MP2 level and the single-point relative energies at the CCSD(T) level are shown in Table 3. The relative energy between the bridged and anti forms of the C_2H_4I• radical is about 3 kcal/mol. This energy difference is of the same order as the energy difference between the anti and gauche conformers of the parent molecule $C_2H_4I_2$ (Supporting Information Table 1S).

Final Products. Table 4 shows the relative energies of the reaction intermediates and products as compared to the parent molecule $C_2H_4I_2$ in the ground state. The bridged haloethyl radical C_2H_4I• + I•, generated from the decay of the excited parent molecule $C_2H_4I_2$*, is initially excited with an excess energy of 45.906 kcal/mol in methanol. Since dissociation of the remaining β-carbon−halogen bond to form C_2H_4 + I• requires an energy input of only 4.391 kcal/mol in the gas phase and 5.212 kcal/mol in methanol, further dissociation is possible. Dissociation of C_2H_4I• by secondary C−I bond breakage might be less efficient in solution than in the gas phase due to vibrational cooling. However, vibrational energy transfer to the solvent may not completely suppress secondary dissociation, because the distribution of internal vibrational energy in the haloethyl radicals is fairly broad.[43,44] The I_2 molecule lies 43.193 kcal/mol lower in energy than two free iodine atoms in methanol. If the secondary dissociation reaction occurs, C_2H_4 + I_2 can be formed directly without energy barrier, as shown in Figure 5. The secondary dissociation is the most important channel in the photochemical reactions of $C_2F_4I_2$ in the gas phase,[21] and the photodissociation studies on $C_2F_4I_2$ and $C_2H_4I_2$ in solution also suggested the secondary dissociation mechanism.[45]

The solvation cage may contain the liberated iodine atom within the interaction distance of the remaining iodine on C_2H_4I• and lead to the formation of a new species. As shown in Figure 5, the interaction of the free iodine atom with the haloethyl radical can form a C_2H_4I-I isomer. The scan along the I−I distance of the isomer shows that there is no energy barrier for the transition from the bridged C_2H_4I• + I to the C_2H_4I-I isomer. The calculated results are shown in Supporting Information Figure 2S.

The C_2H_4I-I isomer has a significant interaction between the C_2H_4 moiety and the I_2 group and is lower in energy than C_2H_4 + I_2 by 1.480, 1.119, and 1.411 kcal/mol in the gas phase, methanol, and cyclohexane, respectively. The geometry of the C_2H_4I-I isomer is shown in Figure 6. The isomer has C_{2v} symmetry, with an I−I bond length of 2.747 Å in methanol (2.733 Å in the gas phase and 2.737 Å in cyclohexane). Compared with the C−I bond length 3.107 Å of the C_2H_4I• radical, the C−I bond length of the C_2H_4I-I isomer is elongated to 3.273 Å in methanol, which indicates a weaker interaction than that in the bridged C_2H_4I•. Due to the long distance between the iodine and carbon atoms, the C_2H_4I-I isomer might be considered as an $I_2-C_2H_4$ van der Waals (vdW) complex. The LUMO and part of the valence molecular orbital depictions of the isomer are shown in Supporting Information Figure 1S. The HOMO-5 shows molecular orbital overlap between the I_2 and C_2H_4 groups. Following the molecular orbital definition,[46] the "overlap" implies covalent character rather than weak vdW interaction. In this context, the isomer is not a "true" vdW complex such as the He dimer, in which there is no MO with bonding character between two He atoms.

The interatomic distances for ordinary vdW interaction can be estimated by the formula $R = 2\sqrt{R_A R_B} - \Delta R$, where R is the van der Waals (vdW) radius and ΔR is the correction term ($\Delta R = R - R_{min}$ or $\Delta R = R - R_{max}$) of which the value usually does not exceed 0.15 Å.[47] With R_C = 1.7 Å,[48] R_I = 2.13 Å[49] and ΔR = 0.15 Å, the lower limit of the vdW distance between carbon and iodine atoms is calculated to be 3.66 Å, which is 0.39 Å longer than the C−I distance of the C_2H_4I-I isomer. The isomer may still be considered as a vdW complex in a broad sense, when individual identities of the I_2 and C_2H_4 moieties of the isomer are emphasized.

In comparison with the secondary dissociation leading to C_2H_4 + 2I, which is a unique reaction channel in the gas phase, the

TABLE 2: Selected Structural Parameters[a] of the Bridged and Anti Conformers of $C_2H_4I\bullet$ in the Gas Phase and in Solution

		gas phase				in methanol		in cyclohexane	
		ROHF	MP2	B3LYP	CCSD(T)	ROHF	B3LYP	ROHF	B3LYP
$C_2H_4I\bullet$_b	C−C	1.319	1.349	1.343	1.351	1.320	1.348	1.319	1.345
	C−I	4.138	3.129	3.149	3.285	4.144	3.107	4.136	3.131
	I−C−C	80.8	77.6	77.7	78.1	80.8	77.5	80.8	77.6
$C_2H_4I\bullet$_a	C−C	1.473	1.463			1.471		1.473	
	C−I	2.205	2.195			2.218		2.209	
	I−C−C	111.7	110.2			111.4		111.7	

[a] Bond lengths in angstroms and angles in degrees; $C_2H_4I\bullet$_b denotes the bridged form, $C_2H_4I\bullet$_a denotes the anti form; the anti form converges to the bridged form at the B3LYP and CCSD(T) levels.

TABLE 3: Relative Energies (kcal/mol) of the Bridged and Anti Conformers of $C_2H_4I\bullet$ in the Gas Phase and in Solution[a]

	HF	MP2	MP3//MP2	MP4SDQ//MP2	CCSD//MP2	CCSD(T)//MP2
$C_2H_4I\bullet$_b	0	0	0	0	0	0
$C_2H_4I\bullet$_a	7.99	3.04	3.94	3.71	3.46	3.55
	(7.39)		(3.77)	(3.52)	(3.26)	(3.41)

[a] The values in parentheses are the relative energies in methanol solution.

TABLE 4: Relative Energies (kcal/mol) of the Reaction Intermediates and Products in the Gas Phase and in Solution at the B3LYP Level[a]

species	gas phase	in methanol	in cyclohexane
$C_2H_4I_2$	0	0	0
$C_2H_4I\bullet$_b + I•	46.66	45.91	46.34
C_2H_4 + 2I•	51.05	51.12	51.08
C_2H_4I−I	5.75	6.81	6.10
C_2H_4 + I_2	7.23	7.93	7.51

[a] All values are corrected for the zero-point energies.

abstraction reaction becomes an important channel in methanol. The change of reaction pathways in going from the gas phase to the solution phase has been established by both experiment and theory previously.[50,51] According to the PES shown in Figure 5 as well as previous experimental results, the following reaction mechanisms are plausible:

In the gas phase

$$C_2H_4I_2^* \rightarrow C_2H_4I\bullet\_b + I\bullet \rightarrow C_2H_4 + 2I\bullet$$

(secondary dissociation)

In solution

$$C_2H_4I_2^* \rightarrow C_2H_4I\bullet\_b + I\bullet \rightarrow C_2H_4 + 2I\bullet \rightarrow C_2H_4 + I_2$$

(secondary dissociation)

$$C_2H_4I_2^* \rightarrow C_2H_4I\bullet\_b + I\bullet \rightarrow C_2H_4I{-}I \rightarrow C_2H_4 + I_2$$

(abstraction reaction)

where $C_2H_4I\bullet$_b stands for the bridged $C_2H_4I\bullet$. In a highly polar solvent like methanol, the strong interaction between the solute and the solvent can suppress secondary dissociation of the haloethyl radical through vibrational cooling. At the same time, the solvation cage built around the solute molecules increases the interaction between the liberated iodine atom and the haloethyl radical. This solvation effect thus promotes the interaction between $C_2H_4I\bullet$ and I to subsequently form the C_2H_4I−I isomer. Therefore, the abstraction becomes an important reaction channel for $C_2H_4I_2$ in solution. Energetically, the abstraction reaction is more favored than the secondary dissociation. The direct formation of C_2H_4 + I_2 from C_2H_4I + I through an abstraction pathway cannot be excluded. However, since the C_2H_4I−I isomer is 1.119 kcal/mol lower in energy than C_2H_4 + I_2 in methanol, the formation of the C_2H_4I−I isomer is more probable.

At this stage, a full description of the photoinduced reaction of $C_2H_4I_2$, supported by both experiments and our calculations, can be proposed. Ihee et al. showed that the excited $C_2F_4I_2$* molecule decays in a two-step process in the gas phase.[21] An ultrafast C−I bond breakage is followed by a secondary C−I cleavage in the resulting $C_2F_4I\bullet$ radical. Lee et al. and Lou et al. also suggested the occurrence of secondary dissociation in haloethyl radicals.[52−54] We note that according to our calculations the isomer formation is energetically more favored than the secondary dissociation even in the gas phase, as shown in Figure 5. However, in a typical gas phase experiment, it is unlikely that the free iodine will encounter the C_2H_4I radical and have a chance to form the isomer. Åkesson et al. suggested in their study of $C_2H_4I_2$ in acetonitrile solutions that both secondary dissociation and abstraction channels are possible and that the process might be dominated by secondary dissociation in the $C_2H_4I\bullet$ radical.[45] In contrast, our recent time-resolved X-ray diffraction study of $C_2H_4I_2$ in methanol[26] revealed that the formation of C_2H_4 + 2I is negligible within the experimental time resolution of 100 ps. Instead, the C_2H_4I−I isomer appears at ∼100 ps, peaks around ∼10 ns, and persists until μs. The results from time-resolved X-ray diffraction are consistent with the conclusion drawn from calculations, that the abstraction is energetically more favored than the secondary dissociation. The measured I−I distance 2.75 Å is also in good agreement with the calculated value 2.747 Å at the B3LYP level. The C_2H_4I−I isomer eventually dissociates into C_2H_4 + I_2, which is 1.119 kcal/mol uphill on the energy surface. Therefore, this final step is entropy driven.[26] The scan calculation along the C−I coordinate of the C_2H_4I−I isomer in Supporting Information Figure 3S shows that no transition state exists between the isomer and C_2H_4 + I_2.

The I_3^- ion, with an absorption maximum at 362 nm, was formed on longer time scales in previous studies of the solution $C_2H_4I_2/CH_3CN$.[45] This species is also observed in our study of $C_2H_4I_2/CH_3OH$,[26] on a time scale of hours. As shown in Figure 6, I_3^- optimized at the B3LYP/6-311+G(d) level has a linear structure with an I−I bond length of 3.011 Å in the gas phase (2.999 Å in methanol and 3.003 Å in cyclohexane).

The Ground and Excited State Potential Energy Surfaces (PESs) of $C_2H_4I_2$ and Vertical Excitation Energy. TD-DFT has proven to be a reliable method for computing transition energies and oscillator strengths.[55,56] The vertical excitation energies and oscillator strengths of the parent molecules $C_2H_4I_2$_anti, intermediate $C_2H_4I\bullet$_bridged, and the C_2H_4I−I isomer in the gas phase and in solution were calculated with the TD-B3LYP method, and the results are shown in Table 5 and Supporting Information Table 6S.

The calculated absorption peak of $C_2H_4I_2$ in methanol is at 269 nm, blue shifted by 2 nm as compared to that in the gas

TABLE 5: Calculated Absorption (nm) and Oscillator Strengths (in Parentheses) of $C_2H_4I_2$ at Different Excited States in the Gas Phase and in Solution at the TD-B3LYP Level

	$C_2H_4I_2$ (anti)		
excited states	gas phase	in methanol	in cyclohexane
1	320 (0)	316 (0)	318 (0)
2	315 (0)	311 (0)	314 (0)
3	312 (0)	309 (0)	311 (0)
4	309 (0)	306 (0)	308 (0)
5	278 (0)	276 (0)	277 (0)
6	271 (0.0005)	270 (0.0002)	271 (0.0003)
7	**271 (0.0355)**	**269 (0.0387)**	**270 (0.0369)**
8	270 (0)	268 (0)	269 (0)
9	248 (0)	248 (0)	248 (0)
10	243 (0)	239 (0)	242 (0)
11	242 (0)	237 (0)	240 (0)
12	238 (0.0127)	234 (0)	236 (0.0127)
13	238 (0)	233 (0.0126)	236 (0)
14	235 (0)	230 (0)	233 (0)
15	233 (0)	229 (0)	231 (0)

phase. In comparison with the experimental absorption peak at 261 nm, an empirical wavelength scaling of 0.97 is needed between theory and experiment. The maximum of I_2 absorption in the visible range calculated at the TD-B3LYP level is 553 nm in the gas phase, identical to the experimental value.[57] No experimental transient absorption spectra for the bridged $C_2H_4I\bullet$ radical and the C_2H_4I-I isomer are available for comparison, but the calculated absorptions and oscillator strengths of the bridged $C_2H_4I\bullet$ radical and the C_2H_4I-I isomer are shown in Supporting Information Table 6S.

The excited PESs of $C_2H_4I_2$ along the r(C−I) bond-stretching coordinate were calculated using the TD-B3LYP method with the same basis sets as described above. Figure 7 shows the various excited states of the PES. Under 267 nm laser excitation (4.65 eV), the $C_2H_4I_2$ molecule is promoted to the seventh excited state (^1B_u state). The excited molecule will at first instance preserve its ground state structure and then relax on the ^1B_u energy curve to form a hot $C_2H_4I_2$* molecule with a greater C···I distance. The subsequent transformations are the dissociation reaction through $C_2H_4I_2^* \rightarrow C_2H_4I\bullet + I\bullet$ and the fast recombination $C_2H_4I_2^* \rightarrow C_2H_4I_2$ due to the surrounding solvent molecules.

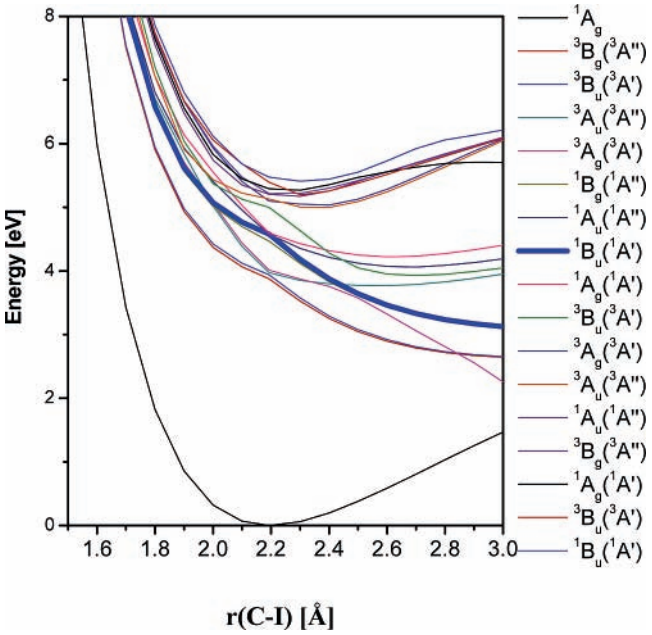

Figure 7. Ground and excited state potential energy surfaces of $C_2H_4I_2$ along the r(C−I) bond-stretching coordinate. The seventh excited state (^1B_u) is plotted thicker (blue) to highlight the dissociation PES of the $C_2H_4I_2$ molecule excited with 267 nm. The C_{2h} symmetry of the ground state structure breaks as the C−I distance becomes longer; the values in parentheses show the C_s group term symbols.

The stretching coordinate at r(C−I) = 3 Å is the point where the restricted DFT singlet ground state breaks down to the unrestricted one, and the TD-DFT single-point energy calculation starts to produce negative excitation energies. For this reason, the excited PESs at r(C−I) > 3 Å are not shown.

4. Conclusion

The photodissociation reaction process of $C_2H_4I_2$ in the gas phase and in solution has been investigated using ab initio and DFT methods. The bridged conformer of the $C_2H_4I\bullet$ radical, which lies about 3 kcal/mol lower in energy than the anti form, is dominant both in the gas phase and in the solution phase. The excited $C_2H_4I_2$* dissociates in a two-step process: in the gas phase, initial C−I bond rupture is followed by secondary cleavage of the C−I bond in the haloethyl radical $C_2H_4I\bullet$, whereas, in solution, the abstraction is a more important process than the secondary dissociation and becomes a major pathway. The C_2H_4I-I isomer, which is a covalently bonded molecule with a lower energy than $C_2H_4 + I_2$, is formed through the interaction of $C_2H_4I\bullet$ with $I\bullet$. The ground state structure of 1,2-diiodoethane in methanol was experimentally determined by static X-ray scattering and compared with the theoretical values. The measured structure is in good agreement with the one predicted by theory.

Acknowledgment. The authors would like to thank Dr. Jim Hess for help in some of the calculations and Veijo Honkimaki and Thomas Buslap for assistance with the high-resolution experiment on beamline ID15. This work was supported by the EU grants FAMTO (HPRI-CT-1999-50004) and FLASH (FP6-503641) and by a grant from the Nano R&D Program of the Korea Science and Engineering Foundation (2005-02638) awarded to H.I.

Supporting Information Available: Tables showing the total energies after zero-point energy (ZPE) correction and relative energies of the different stationary points of $C_2H_4I_2$ in the rotational PES in the gas phase, in methanol, and in cyclohexane calculated at the B3LYP level; optimized structural parameters and the *XYZ* coordinates of the species in Figure 4 at the B3LYP level; calculated vibrational frequencies and IR intensities of the different species on the rotational PES of 1,2-diiodoethane in the gas phase and in methanol at the B3LYP level, and in comparison with experimental data; optimized structural parameters and *XYZ* coordinates of the species in Figure 6 at the B3LYP level; calculated vibrational frequencies and IR intensities of the different species shown in Figure 6 in the gas phase and in methanol at the B3LYP level; calculated absorptions and oscillator strengths of $C_2H_4I\bullet$_bridged and the C_2H_4I-I isomer at different excited states in the gas phase and in solution at the TD-B3LYP level; and calculated Natural Population Analysis (NPA) charges for the C_2H_4I-I isomer and figures showing HOMO, LUMO, and valence molecular orbital depictions of the C_2H_4I-I isomer; the optimized PES along the I−I distance of the C_2H_4I-I isomer; and the optimized PES along the C−I distance of the C_2H_4I-I isomer. This material is available free of charge via the Internet at http://pubs.acs.org.

References and Notes

(1) Kochi, J. K. *Free Radicals*; John Wiley & Sons: New York, 1973; Vol. II.

(2) Beckwith, A. L. J.; Ingold, K. U. *Free-Radical Rearrangements;* Mayo, P. d., Ed.; Academic Press: New York, 1980.
(3) Goering, H. L.; Abell, P. I.; Aycock, B. F. *J. Am. Chem. Soc.* **1952**, *74*, 3588.
(4) Thaler, W. *J. Am. Chem. Soc.* **1963**, *85*, 2607.
(5) Skell, P. S.; Tuleen, D. L.; Readio, P. D. *J. Am. Chem. Soc.* **1963**, *85*, 2849.
(6) Tanner, D. D.; Darwish, D.; Mosher, M. W.; Bunce, N. J. *J. Am. Chem. Soc.* **1969**, *91*, 7398.
(7) Traynham, J. G.; Lee, Y. S. *J. Am. Chem. Soc.* **1974**, *96*, 3590.
(8) Chambers, R. D., Ed. *Organofluorine Chemistry*; Springer-Verlag: Berlin, 1997.
(9) Kerr, J. A. *Handbook of Biomolecular and Termolecular Gas Reactions*; CRC Press: Boca Raton, FL, 1981.
(10) Patai, S.; Rappoport, Z. *Supplement D2 The Chemistry of Halides, Pseudo-Halides, and Azides*; John Wiley & Sons: New York, 1995; Part 2.
(11) Nonebel, D. C.; Tedder, J. M.; Walton, J. C. *Radicals*; Cambridge University Press: Cambridge, U.K., 1997.
(12) Knyazev, V. D.; Bencsura, A.; Dubinsky, I. A.; Gutman, D. *J. Phys. Chem.* **1995**, *99*, 230.
(13) Pilgrim, J. S.; Taatjes, C. A. *J. Phys. Chem. A* **1997**, *101*, 4172.
(14) Misochko, E. Y.; Benderskii, A. V.; Wight, C. A. *J. Phys. Chem.* **1996**, *100*, 4496.
(15) Cramer, C. J. *J. Org. Chem.* **1991**, *56*, 5229.
(16) Engels, B.; Peyerimhoff, S. D.; Skell, P. S. *J. Phys. Chem.* **1990**, *94*, 1267.
(17) Bernardi, F.; Bottoni, A.; Canepa, C.; Olivucci, M.; Robb, M. A.; Tonachini, G. *J. Org. Chem.* **1997**, *62*, 2018.
(18) Kambanis, K. G.; Lazarou, Y. G.; Papagiannakopoulos, P. *Chem. Phys. Lett.* **1997**, *268*, 498.
(19) Eliel, E. L.; Allinger, N. L.; Angyal, S. G.; Morrison, G. A. *Conformational Analysis*; Wiley-Interscience: New York, 1966.
(20) Plech, A.; Wulff, M.; Bratos, S.; Mirloup, F.; Vuilleumier, R.; Schotte, F.; Anfinrud, P. A. *Phys. Rev. Lett.* **2004**, *92*, 125505.
(21) Ihee, H.; Lobastov, V. A.; Gomez, U. M.; Goodson, B. M.; Srinivasan, R.; Ruan, C. Y.; Zewail, A. H. *Science* **2001**, *291*, 458.
(22) Neutze, R.; Wouts, R.; Techert, S.; Davidsson, J.; Kocsis, M.; Kirrander, A.; Schotte, F.; Wulff, M. *Phys. Rev. Lett.* **2001**, *87*, 195508.
(23) (a) Ihee, H.; Kua, J.; Goddard, W. A., III; Zewail, A. H. *J. Phys. Chem. A* **2001**, *105*, 3623. (b) Ihee, H.; Zewail, A. H.; Goddard, W. A., III. *J. Phys. Chem. A* **1999**, *103*, 6638.
(24) Dixon, D. A.; Matsuzawa, N.; Walker, S. C. *J. Phys. Chem.* **1992**, *96*, 10740.
(25) Cheng, Y. P.; Zheng, X. M.; Phillips, D. L. *Asian J. Spectrosc.* **1998**, *2*, 62.
(26) Ihee, H.; Lorenc, M.; Kim, T. K.; Kong, Q. Y.; Cammarata, M.; Lee, J. H.; Wulff, M. *Science* **2005**, *309*, 1223.
(27) Warren, B. E. *X-ray Diffraction*; Dover: New York, 1990.
(28) Nielsen, J. A.; McMorrow, D. *Elements of Modern X-ray Physics*; John Wiley & Sons, Ltd: West Sussex, England, 2001.
(29) Soper, A.; Luzar, A. *J. Chem. Phys.* **1992**, *97*, 1320.
(30) Plech, A.; Randler, R.; Wulff, M.; Mirloup, F.; Vuilleumier, R. *J. Phys.: Condens. Matter* **2003**, *15*, 137.
(31) (a) Hajdu, F. *Acta Crystallogr.* **1972**, *28*, 250. (b) Pálinkás, G. *Acta Crystallogr.* **1973**, *29*, 10.
(32) Frisch, M. J.; Trucks, G. W.; Schlegel, H. B.; Scuseria, G. E.; Robb, M. A.; Cheeseman, J. R.; Montgomery, Jr., J. A.; Vreven, T.; Kudin, K. N.; Burant, J. C.; Millam, J. M.; Iyengar, S. S.; Tomasi, J.; Barone, V.; Mennucci, B.; Cossi, M.; Scalmani, G.; Rega, N.; Petersson, G. A.; Nakatsuji, H.; Hada, M.; Ehara, M.; Toyota, K.; Fukuda, R.; Hasegawa, J.; Ishida, M.; Nakajima, T.; Honda, Y.; Kitao, O.; Nakai, H.; Klene, M.; Li, X.; Knox, J. E.; Hratchian, H. P.; Cross, J. B.; Bakken, V.; Adamo, C.; Jaramillo, J.; Gomperts, R.; Stratmann, R. E.; Yazyev, O.; Austin, A. J.; Cammi, R.; Pomelli, C.; Ochterski, J. W.; Ayala, P. Y.; Morokuma, K.; Voth, G. A.; Salvador, P.; Dannenberg, J. J.; Zakrzewski, V. G.; Dapprich, S.; Daniels, A. D.; Strain, M. C.; Farkas, O.; Malick, D. K.; Rabuck, A. D.; Raghavachari, K.; Foresman, J. B.; Ortiz, J. V.; Cui, Q.; Baboul, A. G.; Clifford, S.; Cioslowski, J.; Stefanov, B. B.; Liu, G.; Liashenko, A.; Piskorz, P.; Komaromi, I.; Martin, R. L.; Fox, D. J.; Keith, T.; Al-Laham, M. A.; Peng, C. Y.; Nanayakkara, A.; Challacombe, M.; Gill, P. M. W.; Johnson, B.; Chen, W.; Wong, M. W.; Gonzalez, C.; Pople, J. A. Gaussian 03, Revision C.02; Gaussian, Inc.: Wallingford, CT, 2004.
(33) Pople, J. A.; Head-Gordon, M.; Raghavachari, K. *J. Chem. Phys.* **1987**, *87*, 5968.
(34) Becke, A. D. *J. Chem. Phys.* **1993**, *98*, 5648.
(35) Lee, C.; Yang, W.; Parr, R. G. *Phys. Rev. B* **1988**, *37*, 785.
(36) McLean, A. D.; Chandler, G. S. *J. Chem. Phys.* **1980**, *72*, 5639.
(37) Stromberg, A.; Gropen, O.; Wahlgren, U. *J. Comput. Chem.* **1983**, *4*, 181.
(38) Glukhovtsev, M. N.; Pross, A. *J. Chem. Phys.* **1995**, *103*, 1878.
(39) Foresman, J. B.; Keith, T. A.; Wiberg, K. B.; Snoonian, J.; Frisch, M. J. *J. Phys. Chem.* **1996**, *100*, 16098.
(40) Stratmann, R. E.; Scuseria, G. E.; Frisch, M. J. *J. Chem. Phys.* **1998**, *109*, 8218.
(41) Ukaji, T.; Kuchitsu, K. *Bull. Chem. Soc. Jpn.* **1966**, *39*, 2153.
(42) (a) Onsager, L. *J. Am. Chem. Soc.* **1936**, *58*, 1486. (b) Kirkwood, J. G. *J. Chem. Phys.* **1934**, *2*, 351.
(43) Khundkar, L. R.; Zewail, A. H. *J. Chem. Phys.* **1990**, *92*, 231.
(44) Zhong, D.; Ahmad, S.; Zewail, A. H. *J. Am. Chem. Soc.* **1997**, *119*, 5978.
(45) Rasmusson, M.; Tarnovsky, A. N.; Pascher, T.; Sundström, V.; Åkesson, E. *J. Phys. Chem. A* **2002**, *106*, 7090.
(46) Pavel, H.; Rudolf, Z. *Chem. Rev.* **1988**, *88*, 871.
(47) Zefirov, Y. V.; Zorkii, P. M. *Russ. Chem. Rev.* **1989**, *58*, 421.
(48) Huheey, J. E.; Keiter, E. A.; Keiter, R. L. *Inorganic Chemistry: Principles of Structure and Reactivity*, 4th ed.; Harper Collins College Publishers: New York, 1993; p 292.
(49) Nyburg, S. C.; Faerman, C. H. *Acta Crystallogr., Sect. B* **1985**, *41*, 274.
(50) Chuang, T. J.; Hoffman, G. W.; Eisenthal, K. B. *Chem. Phys. Lett.* **1974**, *25*, 201.
(51) Castejon, H.; Wiberg, K. B. *J. Am. Chem. Soc.* **1999**, *121*, 2139.
(52) Nathanson, G. M.; Minton, T. K.; Shane, S. F.; Lee, Y. T. *J. Chem. Phys.* **1989**, *90*, 6157.
(53) Minton, T. K.; Felder, P.; Brudzynski, R. J.; Lee, Y. T. *J. Chem. Phys.* **1984**, *81*, 1759.
(54) Wang, G. J.; Zhang, H.; Zhu, R. S.; Han, K. L.; He, G. Z.; Lou, N. Q. *Chem. Phys.* **1999**, *241*, 213.
(55) Jamorski, C.; Casida, M. E.; Salahub, D. R. *J. Chem. Phys.* **1996**, *104*, 5134.
(56) Petersilka, M.; Gossmann, U. J.; Gross, E. K. U. *Phys. Rev. Lett.* **1996**, *76*, 1212.
(57) Steinfeld, J. I.; Jones, L.; Lesk, M.; Klemperer, W. *J. Chem. Phys.* **1965**, *42*, 25.